KU LEUVEN

ExampleSat

Pointing Performance Analysis

January 25, 2018

Contents

1 SUMMARY

This document describes the pointing analysis simulation and results for the Example mission. The simulation was run using the input values provided by the satellite integrator.

The simulation environment used in this analysis is built in Matlab/Simulink. The environment consists of an attitude propagator and orbit propagator. This is linked to the simulated control loop of the KUL ADCS, with all estimation and control modes included. The desired attitude for pointing modes such as Nadir and Sun pointing are calculated autonomously. The simulations incorporate the major noise sources that can be found in CubeSat missions, such as disturbance torques, sensor noise and actuator noise.

1.1 DETUMBLING

Several control modes are analysed. First, detumbling scenarios with varying initial tumble rates are analysed. We verify that the rotational rates go down for all realistic initial rates. The energy consumption during the detumbling scenarios is given to allow energy budget assessment right after the launch.

From the detumbling analysis, we can conclude that the satellite can reduce its rotational rates, even with worst case initial tumble rates.

1.2 3-AXIS CONTROL

The 3-axis control scenario, which is the nominal scenario, is analysed in detail. The attitude determination performance, attitude control performance and power consumption is analysed for different ADCS modes. The most important result is that of the 3 Reaction Wheel (RW) with Star Tracker mode, since that is the nominal mode. The other modes, either using only 1 RW or not using the star tracker are fallback or energy-saving modes.

The pointing performance in the 3-axis scenario is validated in two different ways. For all simulation runs of one mode, we calculate the root mean square pointing and knowledge error for all three axes. The mean of this is taken as the final RMS value. On top of this, we check whether the pointing/knowledge error on each of the axes remains below the desired maximum error (given by the integrator), for each time step. This way, we can calculate the percentage of time that all three axes comply with the desired maximum error. These calculations are done for the pointing and knowledge error, both in and outside of eclipse, resulting in 4 scenarios.

1.2.1 INERTIAL POINTING

The performance results for the “3RW, with star tracker” mode during Inertial pointing are given in table 1.

Table 1: Pointing Performance during Inertial pointing

	Knowledge accuracy outside eclipse		Knowledge accuracy inside eclipse	
Mode	RMS value (deg)	% time met	RMS value (deg)	% time met
Three RWs, Star Tracker	0.036104	100	0.033528	100
	Pointing accuracy outside eclipse		Pointing accuracy inside eclipse	
Mode	RMS value (deg)	% time met	RMS value (deg)	% time met
Three RWs, Star Tracker	0.15101	99.6554	0.14752	100

Thanks to the star tracker, which allows to determine the attitude both inside and outside of eclipse, there is little difference between the performance in and outside of eclipse. The RMS pointing error outside of eclipse is equal to 0.15101 deg, and the desired pointing accuracy is met during 99.6554% of the time. The RMS knowledge error outside of eclipse is 0.036104 deg, resulting in meeting the requirement for 100% of the time.

From the Inertial pointing analysis, we can conclude that the knowledge and pointing requirements can be met using the KUL ADCS.

1.2.2 ZENITH POINTING

PAGES LEFT OUT IN THE EXAMPLE DOCUMENT

2 INTRODUCTION

The pointing performance analysis is a crucial component in a spacecraft mission analysis. The pointing performance of a spacecraft has an important and direct impact on power generation, downlink capacity and payload performance.

In the following document, the pointing performance of the CubeSat with the KU Leuven ADCS is simulated using a highly detailed simulation environment. We first describe the simulation environment, including noises and disturbances. We outline the algorithms that are implemented and the parameters that are used. The pointing performance of the satellite is then simulated for a wide variety of situations. The results that are presented in this document allow to analyse the spacecraft pointing performance with different pointing modes, different estimator and control settings and within and out of eclipse.

3 SIMULATION ENVIRONMENT

This section describes the simulation environment that is used to simulate the ADCS performance. This environment is implemented in Matlab/Simulink and describes the entire ADCS functionality in high detail.

3.1 OVERVIEW

The overall simulation environment is represented in figure 1. The ADCS is in essence a feedback loop. The sensors measure the attitude of the spacecraft and their output is passed on to the estimators. Two estimators that fuse the sensor information are implemented. The Extended Kalman Filter outputs both the estimated attitude and rotational rate. The Kalman Rate Filter outputs the rotational rate. This estimated state of the satellite is compared to the desired state. This desired state can be calculated autonomously by the ADCS, when a pointing mode (e.g. Earth Pointing) is set. The difference between estimated and desired state is sent to the controllers, who determine the action that must be undertaken by the actuators, to orient the spacecraft as desired.

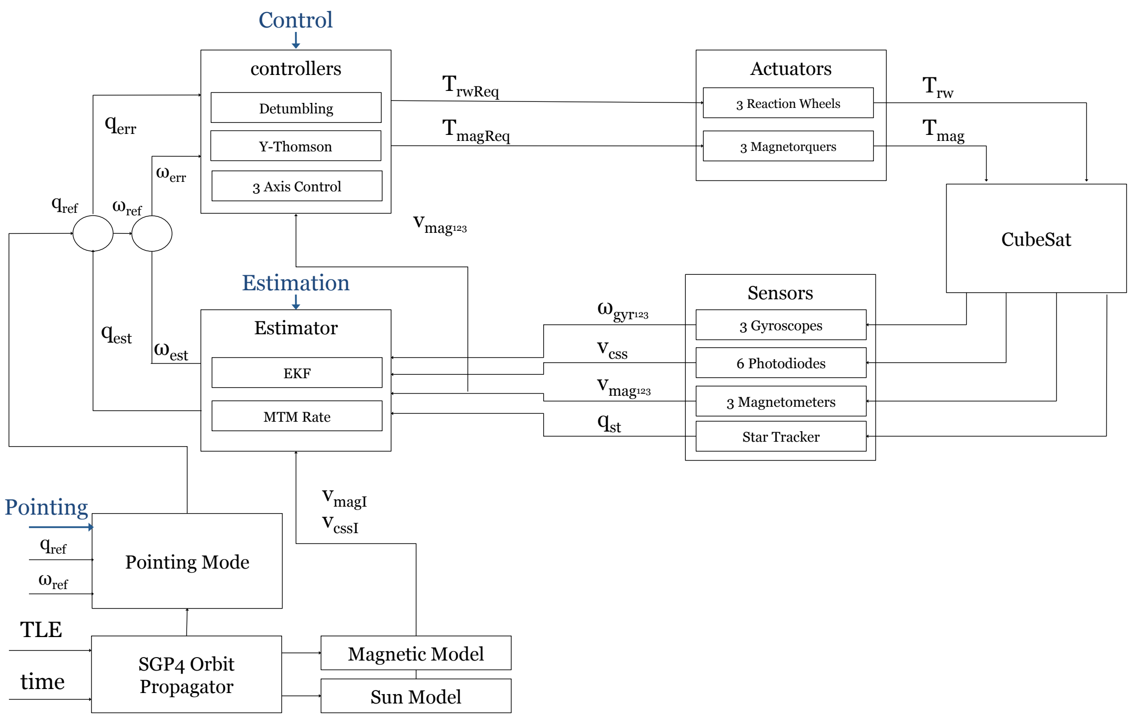

Figure 1: The ADCS Simulation Environment.

3.2 ORBIT PROPAGATION

PAGES LEFT OUT IN THE EXAMPLE DOCUMENT

3.3 MAGNETIC AND SOLAR MODEL

PAGES LEFT OUT IN THE EXAMPLE DOCUMENT

3.4 POINTING MODE

The ADCS has several pointing modes which can be easily switched throughout the mission. The ADCS autonomously determines the action it needs to take to maintain the pointing mode.

3.4.1 INERTIAL POINTING

In Inertial Pointing, the satellite receives a quaternion as input and will continuously point in that attitude.

3.4.2 NADIR POINTING

When Nadir Pointing is selected, a chosen axis will be pointing along the vector towards the center of the Earth. This pointing mode can be used e.g. for Earth observation satellites that want to point a payload towards the center of the Earth. Since only one vector is specified in Earth Pointing, there is a degree of freedom around that vector. At this point, the degree of freedom is used to minimize drag. This can however be changed if wanted.

3.4.3 ZENITH POINTING

When Earth Pointing is selected, a chosen axis will be pointing along the vector towards the Earth, but in the direction away from Earth. Since only one vector is specified in Zenith Pointing, there is a degree of freedom around that vector. At this point, the degree of freedom is used to minimize drag. This can however be changed if wanted.

3.4.4 SOLAR POINTING

When Sun Pointing is selected, a chosen axis will be pointing along the vector towards the Sun. This pointing mode can be used e.g. to maximize power generation with solar panels. Since only one vector is specified in Sun Pointing, there is a degree of freedom around that vector. At this point, the degree of freedom is used to minimize drag. This can however be changed if wanted.

3.4.5 EARTH LOCATION POINTING

When Earth Location Pointing is selected, a chosen axis will be pointing towards a location on Earth. The location is specified using LLA coordinates. This pointing mode can be used e.g. to point a payload to a location of interest on Earth or to point antennas to a ground station. Since only one vector is specified in Earth Location Pointing, there is a degree of freedom around that vector. At this point, the degree of freedom is used to minimize drag. This can however be changed if wanted.

3.5 ATTITUDE DYNAMICS AND KINEMATICS

The attitude propagator model is shown in figure 2. This model combines the dynamic and kinematic equations of motion of the spacecraft.

3.5.1 DYNAMIC EQUATIONS OF MOTION

The first part of the model holds the dynamic equations of motion which relate the spacecraft rotational velocity ω_s to the torques and momentum. The general equation for this is [6]:

$$I\frac{d\omega_s}{dt} = T - \omega \times h \tag{1}$$

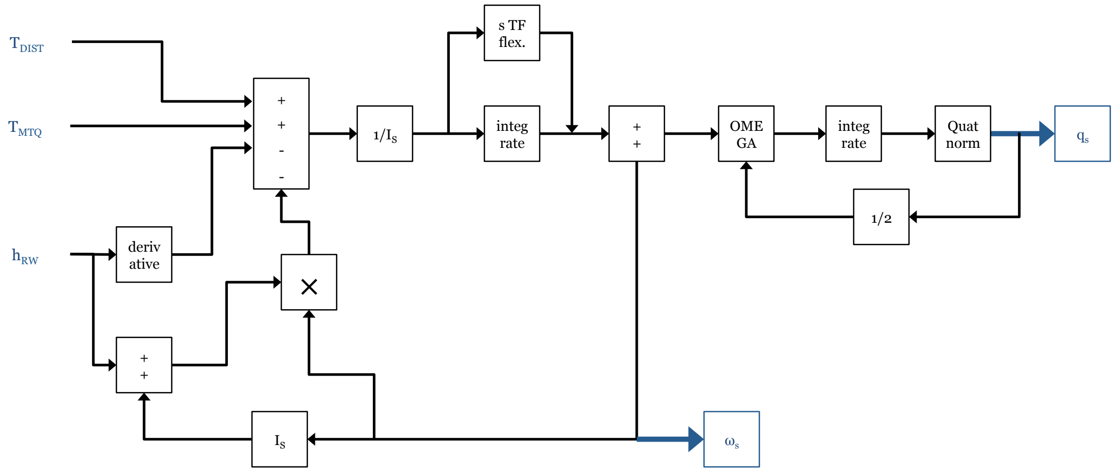

Figure 2: Model of the attitude propagation

Since the ADCS also contains reaction wheels, the momentum term h needs to incorporate both the spacecraft momentum as the reaction wheel momentum, leading to:

$$I\frac{d\omega_s}{dt} = T - \frac{dh_{RW}}{dt} - \omega \times (I\omega + h_{RW}) \tag{2}$$

To clarify this further, the MTQ and disturbance torques are also specified:

$$I\frac{d\omega_s}{dt} = T_{dist} + T_{MTQ} - \frac{dh_{RW}}{dt} - \omega \times (I\omega + h_{RW}) \tag{3}$$

If there are flexible parts in the spacecraft, these are also added in the model. The transfer function obtained in section 3.6 are first converted to obtain the effect of the flexible parts of the spacecraft rotational velocity in stead of rotational angle and are then added to the rigid body rotational velocity.

3.5.2 KINEMATIC EQUATIONS OF MOTION

The kinematic equation of motion is[6]:

$$\frac{dq_s}{dt} = \frac{1}{2}\Omega q_s \tag{4}$$

which can be approximated by

$$q_s(t + \Delta t) = q_s(t) + \frac{1}{2}q_s(t)\Omega\Delta t \tag{5}$$

with:

$$\Omega = \begin{bmatrix} 0 & -\omega_x & -\omega_y & -\omega_z \\ \omega_x & 0 & \omega_z & -\omega_y \\ \omega_y & -\omega_z & 0 & \omega_x \\ \omega_z & \omega_y & -\omega_x & 0 \end{bmatrix} \tag{6}$$

In the end, the quaternion is normalized, to make sure that numerical errors do not add up.
The main results of the attitude propagation are the spacecraft attitude and rotational velocity.

3.6 FLEXIBLE PARTS

In the field of Attitude Determination and Control of CubeSats, one typically assumes that the CubeSat is one rigid structure. In this analysis, we also take into account the effect of flexible parts, such as deployable solar panels and extendable booms. For clarity, the pointing performance is analysed for the spacecraft body, not for the payload at the end of the boom.

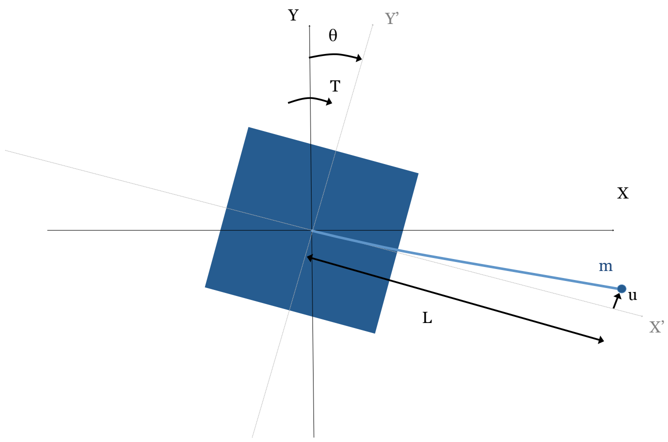

Figure 3: Discrete model of a rigid body spacecraft with a flexible appendage

PAGES LEFT OUT IN THE EXAMPLE DOCUMENT

3.7 TRANSFORMATIONS

PAGES LEFT OUT IN THE EXAMPLE DOCUMENT

3.8 DISTURBANCE TORQUES

Disturbance torques can be divided in two groups [4]:

- **Cyclic**: varying in a sinusoidal manner during an orbit and integrate to zero over an integer number of cycles.
- **Secular**: not periodic or averaging out over an orbit and accumulating with time.

In the following sections, the main disturbance torques acting on the CubeSat will be calculated. Worst-case calculation will be made.

3.8.1 SOLAR PRESSURE

The solar pressure torque T_{sp} is cyclic for earth-oriented spacecraft since the exposed surface varies. A constant exposed surface for solar-oriented spacecraft results in a secular disturbance. Because SIMBA will be earth-oriented for the majority of the mission duration, T_{sp} is considered to be cyclic.

T_{sp} is mostly influenced by the spacecraft geometry, surface properties and center of gravity location. The solar pressure is calculated as [7]:

$$F = \frac{F_s}{c} A_s (1 + q_{sol}) cos(i_{sol}) \tag{7}$$

This force is calculated for each of the sides of the spacecraft, based on the characteristics of the surface and the known vector towards the sun. The torque is obtained by taking the crossproduct with the momentum arm, being the 3D vector from the center of gravity to the center of pressure.

$$T_{sp} = F \times \Delta_{(cp,cg)} \tag{8}$$

3.8.2 GRAVITY GRADIENT

The gravity gradient torque T_{gg} is secular for earth-oriented spacecraft where the angle between the nadir vector and body axis remains constant. A constant external torque is generated since the lower extremities compared to the higher are exposed to higher gravity forces. They become cyclic for inertial pointed spacecraft where the angle is varying. Because SIMBA will be earth-oriented for the majority of the mission duration, $T_{gg}$is considered to be secular.

Besides inertia, T_{gg} is primarily influenced by the orbit altitude and calculated as [7]:

$$T_{gg} = \frac{3\mu_{gg}}{2(R+h)^3}|I_z - I_y|sin(2\theta) \tag{9}$$

This torque is calculated over 3 axes.

3.8.3 MAGNETIC FIELD

The magnetic field disturbance torque T_{mf} is a cyclic disturbance created by the residual spacecraft magnetic dipole D_{mag} $[Am^2]$ (from magnetic material and current loops) which tends to align with the earth magnetic field. T_{mf} has a period of a complete orbit for earth pointing spacecraft and a half when sun pointing.

The magnitude of D_{mag}, orbit altitude and inclination are the main parameters influencing T_{mf} expressed by [7]

$$T_M = D_{mag}B \tag{10}$$

With

$$B = \frac{2M}{(R+h)^3} \tag{11}$$

The main difficulty in calculating the T_{mf} is determining D_{mag}, which is generally obtained by testing. A mean of $\pm$10 loops/PCB or $D_{mag} = 0.05Am^2$ seems to be an acceptable value to incorporate the current loops and magnetic material. A similar value is found when dipole values used in [2], [3], and [1] are averaged, taking into account the number of Units.
The torque is calculated over three axes using the expected magnetic moment of the satellite and the known vector towards the earth's magnetic field.

3.8.4 AERODYNAMIC DRAG

PAGES LEFT OUT IN THE EXAMPLE DOCUMENT

3.9 ACTUATORS

The ADCS has three reaction wheels and three magnetorquers that allow to control the spacecraft attitude with high agility and accuracy.

3.9.1 REACTION WHEELS

The reaction wheels are the actuators within the ADCS that allow full 3-axis control with high accuracy. In essence, the reaction wheels are brushless DC powered flywheels. The reaction wheels control the spacecraft attitude by exchanging momentum with the satellite. When the reaction wheels spin up in one direction, the spacecraft will accelerate in the other rotational direction, due to the principle of conservation of angular momentum. With three reaction wheels on three different axes, full attitude control can be obtained.

PAGES LEFT OUT IN THE EXAMPLE DOCUMENT

3.9.2 MAGNETORQUERS

The magnetorquers are electrical coils that generate a magnetic moment. This magnetic moment interacts with the Earth magnetic field to generate a torque. Magnetorquers do not allow to control the spacecraft attitude fully over three axes.

PAGES LEFT OUT IN THE EXAMPLE DOCUMENT

3.10 SENSORS

The ADCS has a set of different sensors that allow to determine the attitude with high accuracy. The sensors are in general modeled by taking the true measurement and adding white and colored noise to it. The total noise of the absolute sensors was measured in experiments. The total measured noise is split up in one half white and one half colored noise in the simulations. The noise of the gyroscope was measured in an Allan Variance test [5].

PAGES LEFT OUT IN THE EXAMPLE DOCUMENT

4 SIMULATION PARAMETERS

Table 2: Simulation Parameters

Symbol	Description	Value	unit
	Spacecraft		
I_s	The inertia matrix of the spacecraft	$\begin{bmatrix} 0.05 & 0 & 0 \\ 0 & 0.05 & 0 \\ 0 & 0 & 0.025 \end{bmatrix}$	kgm^2
	Flexible Parts		
$m_{boom_{end}}$	Mass at the end of the boom	0.020	kg
$\frac{m_{boom}}{L_{boom}}$	Mass of the boom per length	0.01	$\frac{kg}{m}$
L_{boom}	Boom length	0.3	m
ζ_{boom}	Damping ratio of the boom	0.0125	-
σ_{boom}	Modal eigenvalue of the boom	4	Hz
dir_{boom}	Direction of the boom	plus Y	axis
	Orbit		
$\frac{\dot{n}}{2}$	First time derivative of the mean motion divided by two	$1e-08$	$\frac{rev}{day^2}$
$\frac{\ddot{n}}{6}$	Second time derivative of the mean motion divided by six	0	$\frac{rev}{day^3}$
B^*	BSTAR drag term	-0.006	$\frac{1}{EarthRadii}$
inc	Inclination of the orbit	98	deg
RAAN	Right Ascension of the Ascending Node	40	deg
ecc	Eccentricity of the orbit	0.001	-
AOP	Argument of Perigee	0	deg
MA	Mean Anomaly	0	deg
n	Mean Motion	15	$\frac{rev}{day}$

PAGES LEFT OUT IN THE EXAMPLE DOCUMENT

4.0.1 Coordinate frame

PAGES LEFT OUT IN THE EXAMPLE DOCUMENT

5 CONTROL ALGORITHMS

5.1 DETUMBLING

A B-dot controller is used for detumbling. All three magnetorqures are actuated to reduce the angular rate of the spacecraft.

$$M = -K_{detum}\frac{dB}{dt} \tag{12}$$

5.2 THOMSON SPIN

PAGES LEFT OUT IN THE EXAMPLE DOCUMENT

5.3 3-AXIS CONTROL

PAGES LEFT OUT IN THE EXAMPLE DOCUMENT

6 ESTIMATION ALGORITHMS

6.1 EXTENDED KALMAN FILTER

An extended Kalman Filter is used to estimate the attitude (a quaternion), rotational rate and gyroscope bias. The EKF uses the gyroscope measurements during propagation. There is an update step for each of the attitude sensors. The EKF continues to function when one or more of the sensors is unavailable. If no sensors are available, there is only an update step.

6.1.1 STATE PREDICTION

The EKF uses the kinematic equations in the prediction step.

$$\hat{q}_{k+1}^{-} = \frac{1}{2}\bar{\Omega}(\hat{\omega}_k^{+})\hat{q}_k^{+} \tag{13}$$

With:

$$\bar{\Omega}(\hat{\omega}_k^{+}) = \begin{bmatrix} cos(\frac{1}{2}\left\|\hat{\omega}_k^{+}\right\|\Delta t & -\hat{\Psi}_k^{+T} \\ \hat{\Psi}_k^{+T} & I_{3\times 3}cos(\frac{1}{2}\left\|\hat{\omega}_k^{+}\right\|\Delta t) - [\hat{\Psi}_k^{+}\times] \end{bmatrix} \tag{14}$$

$$\hat{\Psi}_k^{+} = \frac{sin(\frac{1}{2}\left\|\omega_k^{+}\right\|\Delta t)\hat{\omega}_k^{+}}{\left\|\hat{\omega}_k^{+}\right\|} \tag{15}$$

The bias is also estimated in the EKF and the gyroscope input is corrected for this bias.

$$\hat{\omega}_k^{+} = u_k - \hat{\beta}_k^{+} \tag{16}$$

The prediction step does not change the bias.

$$\hat{\beta}_k^{-} = \hat{\beta}_k^{+} \tag{17}$$

PAGES LEFT OUT IN THE EXAMPLE DOCUMENT

6.2 MTM RATE FILTER

PAGES LEFT OUT IN THE EXAMPLE DOCUMENT

Detumbling Performance

7 DETUMBLING PERFORMANCE

When the ADCS is in detumbling mode, it uses the magnetorquers to reduce the rotational rate of the spacecraft. The detumbling mode is typically used after the deployment of the satellite, when it might exhibit high rotational rates. Also when an anomaly, e.g. a power outage, has led to the spinning up of the satellite, the detumbling mode can be used to reduce the spacecraft rotational rates.

The detumbling mode performance was simulated by applying high initial rotational rates to the spacecraft. Five scenarios with different starting rotational rates were used, where scenario 1 represents the rotational rates that can be expected when all reaction wheels decay from maximum spin rate to zero rpm. The simulated rates are shown in the table below:

Table 3: Detumbling scenarios

Name	ω_{init}	Unit
Scenario 1	$(-3, 3, -5)$	$\frac{deg}{s}$
Scenario 2	$(-10, 10, -10)$	$\frac{deg}{s}$
Scenario 3	$(-20, 20, -20)$	$\frac{deg}{s}$
Scenario 4	$(-30, 30, -30)$	$\frac{deg}{s}$
Scenario 5	$(-100, 100, -100)$	$\frac{deg}{s}$

In this control mode, the spacecraft attitude is not controlled, rather the rotational rates are being controlled. The goal of this mode is to reduce the rotational rates of the spacecraft.

7.1 POINTING PERFORMANCE

PAGES LEFT OUT IN THE EXAMPLE DOCUMENT

7.2 KNOWLEDGE PERFORMANCE

PAGES LEFT OUT IN THE EXAMPLE DOCUMENT

7.3 POWER CONSUMPTION

PAGES LEFT OUT IN THE EXAMPLE DOCUMENT

Thomson Spin Performance

8 THOMSON SPIN PERFORMANCE

8.1 KNOWLEDGE PERFORMANCE

PAGES LEFT OUT IN THE EXAMPLE DOCUMENT

8.2 POINTING PERFORMANCE

PAGES LEFT OUT IN THE EXAMPLE DOCUMENT

8.3 POWER CONSUMPTION

PAGES LEFT OUT IN THE EXAMPLE DOCUMENT

Inertial Pointing Performance

9 3-AXIS CONTROL PERFORMANCE: INERTIAL POINTING CASE

In the inertial pointing mode, the ADCS controls the spacecraft to maintain a fixed attitude in the inertial frame. This mode could be used to monitor certain portions of the sky or to point at stars. These simulations start with a maneuver towards a randomly created attitude and the spacecraft then stays oriented in the same way.

The sections below describe the knowledge performance, pointing performance and power consumption in the inertial pointing case. For each of these, Four different ADCS configurations are analysed:

- **One RW, without Star Tracker:** Using a coarse pointing algorithm which requires only one RW and the two MTQs. The star tracker is not powered on.
- **One RW, with Star Tracker:** Using a coarse pointing algorithm which requires only one RW and two MTQs. The star tracker is powered on.
- **Three RWs, without Star Tracker:** A PID-controller using all RWs and all MTQs (for desaturation) is used. The star tracker is not powered on.
- **Three RWs, with Star Tracker:** A PID-controller using all RWs and all MTQs (for desaturation) is used. The star tracker is powered on.

In nominal operation, the ADCS will use three RWs and the star tracker. The other modes are there as a fallback should a component fail. Not using the star tracker will also save power.

Most of the graphs in the next section give an example of one of the simulation runs. These serve to show the overall performance and behavior of the spacecraft in the given mode. At the end, histograms and tables give the overall results over all simulation runs and allow to assess the performance.

The graphs giving the result of one run typically show a certain characteristic (e.g. pointing error) over time. Gray areas in the graphs indicate periods of eclipse. For certain ADCS configurations, behavior inside and out of eclipse will be different.

9.1 KNOWLEDGE PERFORMANCE

The knowledge performance of the ADCS depends on the sensors being used. There will be a difference between the knowledge performance with and without use of the star tracker. The used actuators or control law do not have a significant impact. The knowledge performance is hence analysed for two different cases: with and without star tracker.

9.1.1 THREE RWs WITHOUT STAR TRACKER

When the star tracker is not used, the ADCS determines the attitude based on the magnetometer, photodiode and gyroscope measurements. The magnetometer and photodiode both determine a vector, along the magnetic field and towards the sun respectively. The ADCS requires two vectors to fully determine the attitude. Since the magnetometer is duty cycled with the magnetorquers, this vector might not always be available. More importantly, in eclipse the sun vector will not be observed. During eclipse, the attitude will only be propagated using the gyroscope measurements. Due to drift in the measurements, an accumulating error will arise during eclipse.

9.1.1.1 Analysis of example simulation run

Figure 4 shows the estimation error of the ADCS. This is the difference in degrees between the Kalman Filter estimated attitude and the known true attitude. Outside of eclipse, this error is limited to a few degrees. In eclipse, the pointing knowledge deteriorates quite rapidly due to the fact that the absolute attitude cannot be determined. Once the spacecraft exits eclipse, the pointing knowledge is rapidly restored.

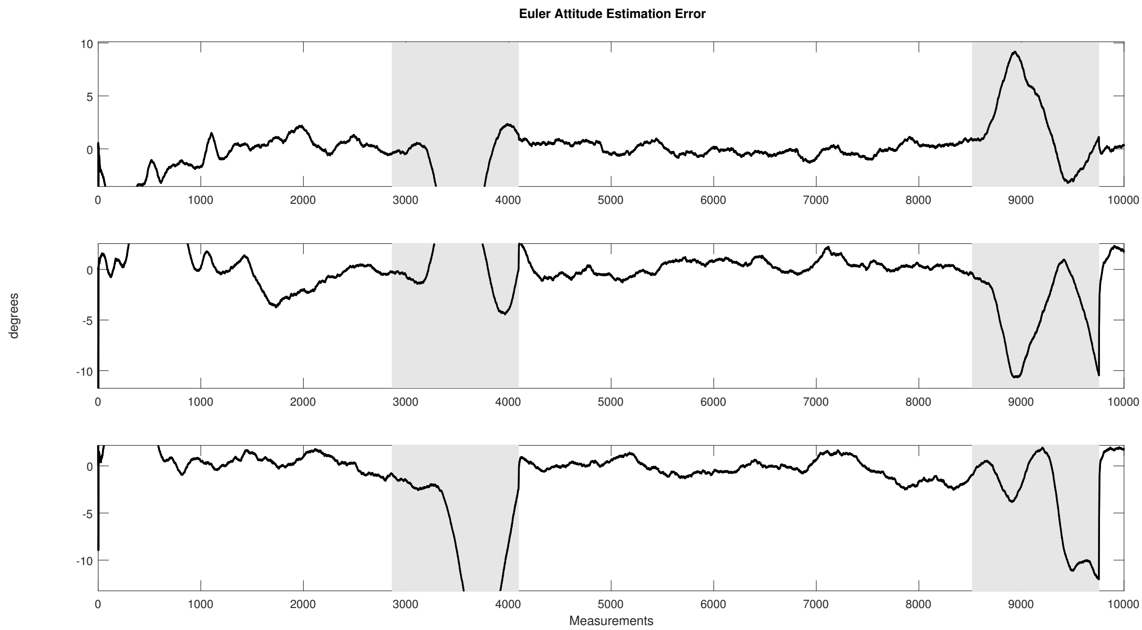

Figure 4: Attitude Estimation Error

In Figure 5, the rate estimation error of the ADCS is shown. These errors are calculated as the difference between the estimated rates and the known true rates. The ADCS can determine the rotational rate of the spacecraft in a number of different ways: (1 Dark Blue) Directly from the raw gyroscope measurements, (2 Black) as an output of the Extended Kalman Filter which also estimates and subtracts the bias and (3 Light Blue) as an output of the MTM rate filter.

The gyroscope measurement error increases over time due to the bias of the star tracker. The Extended Kalman Filter yields the most accurate result. The output of this filter is the measured rate minus the estimated bias, resulting in an estimate that stays closer to the ground truth throughout the entire simulation run. The simple MTM rate filter is a less accurate estimator which should only be used when no other information is available.

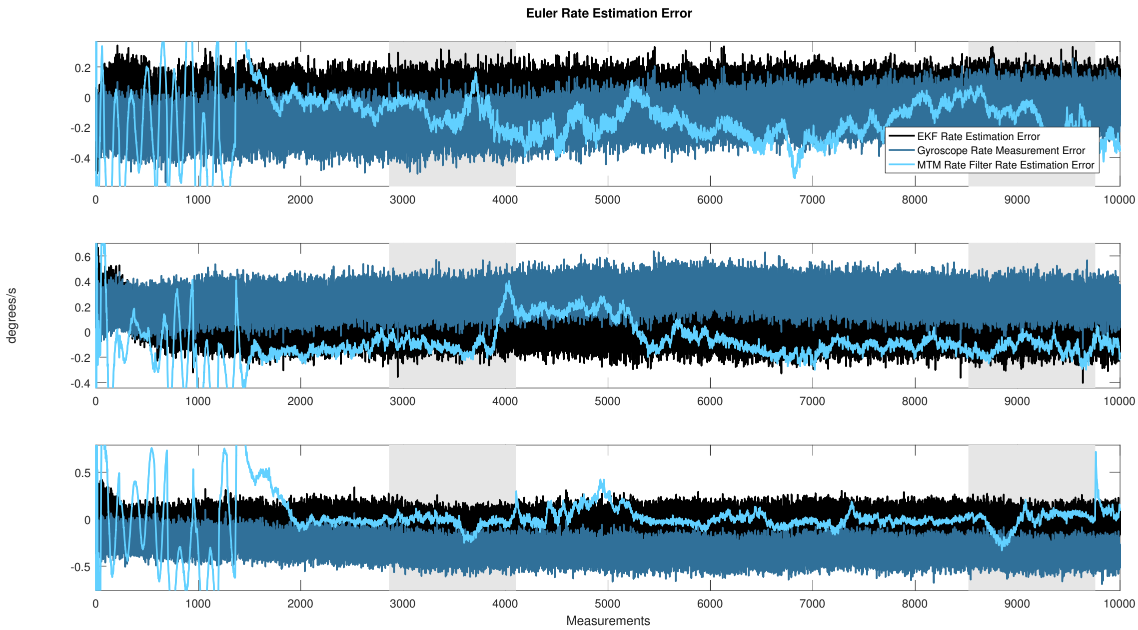

Figure 5: Rate Estimation Error

9.1.1.2 Analysis of all simulation runs

Figure 6 shows a histogram of the knowledge accuracy outside eclipse over all simulation runs in this configuration. For 50% of the time, the knowledge error remains below 1.0867 degrees. The knowledge error remains below 4.1748 degrees for 95% of the time.

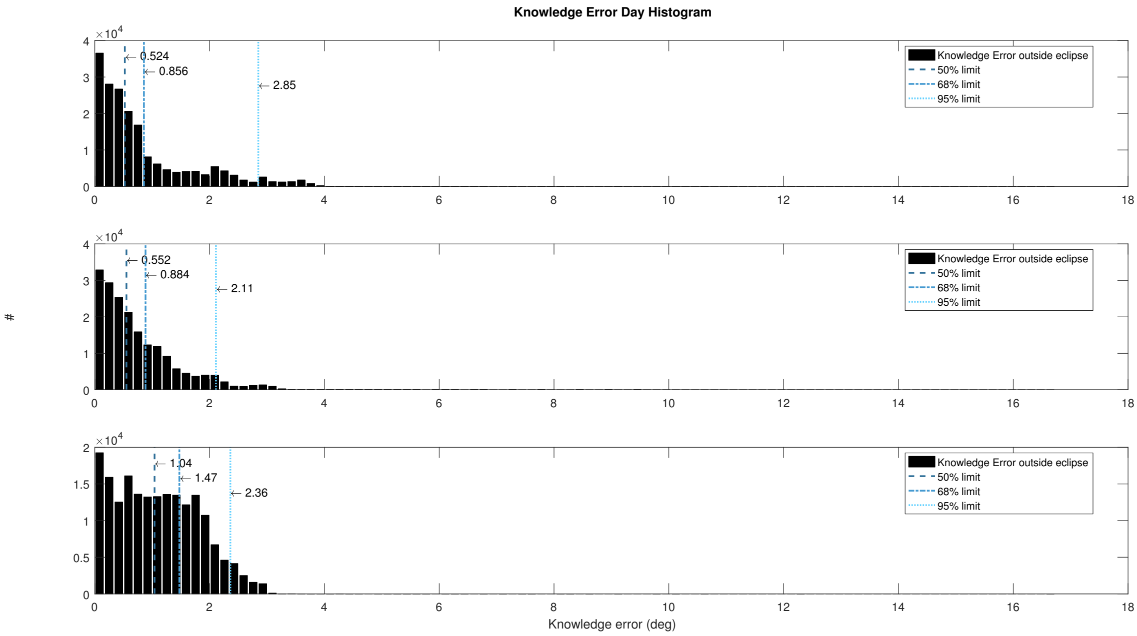

Figure 6: Histogram of the attitude knowledge error outside of eclipse

Figure 7 shows a histogram of the knowledge accuracy within eclipse over all simulation runs in this configuration. For 50% of the time, the knowledge error remains below 3.9168 degrees. The knowledge error remains below 13.9371 degrees for 95% of the time.

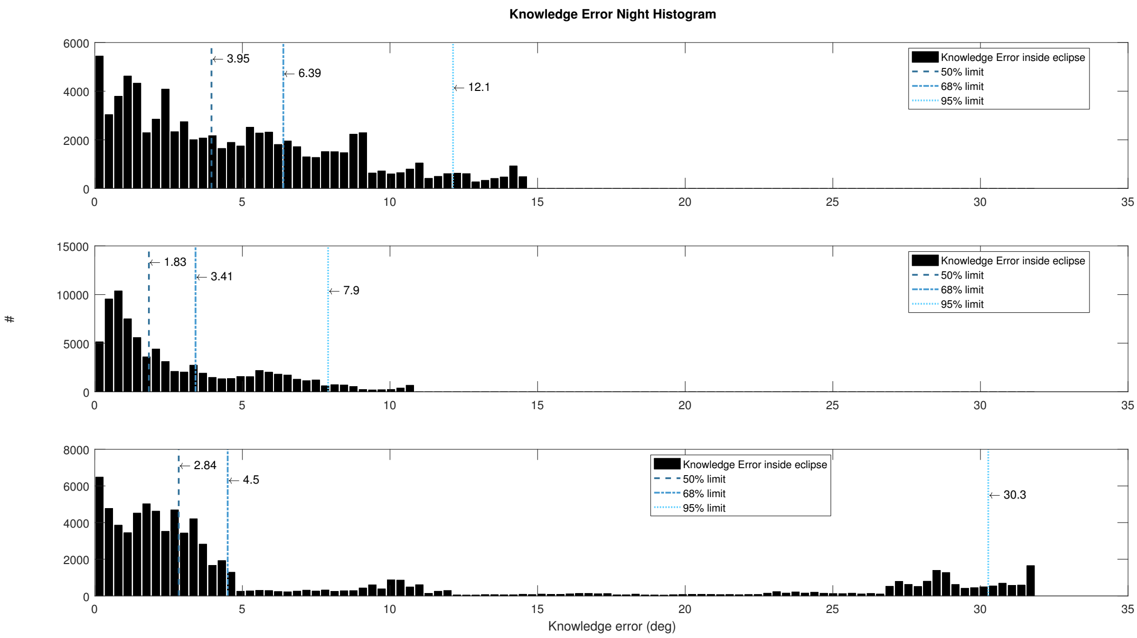

Figure 7: Histogram of the attitude knowledge error within of eclipse

9.1.2 THREE RWs WITH STAR TRACKER

When the star tracker is used, the ADCS determines the attitude based on the star tracker, magnetometer, photodiode and gyroscope measurements. The star tracker functions both within and outside of eclipse and provides full attitude knowledge. Its accuracy is significantly higher than that of the other sensors with a knowledge accuracy in the range of arc seconds. A star tracker yields higher accuracy around the cross-boresight axes than around the optical axis.

9.1.2.1 Analysis of example simulation run

Figure 8 shows the estimation error of the ADCS. This is the difference in degrees between the Kalman Filter estimated attitude and the known true attitude. Both within and outside of eclipse, the attitude is known to within fractions of a degree.

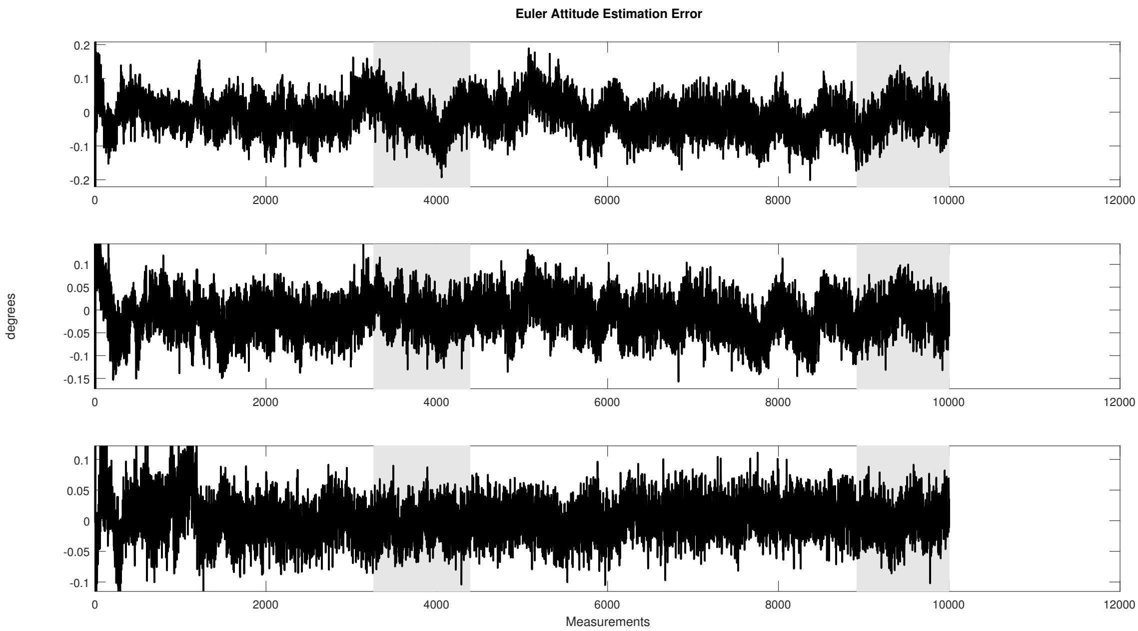

Figure 8: Attitude Estimation Error

In Figure 9, the rate estimation error of the ADCS is shown. These errors are calculated as the difference between the estimated rates and the known true rates. The ADCS can determine the rotational rate of the spacecraft in a number of different ways: (1 Dark Blue) Directly from the raw gyroscope measurements, (2 Black) as an output of the Extended Kalman Filter which also estimates and subtracts the bias and (3 Light Blue) as an output of the MTM rate filter.

The gyroscope measurement error increases over time due to the bias of the star tracker. The Extended Kalman Filter yields the most accurate result. The output of this filter is the measured rate minus the estimated bias, resulting in an estimate that stays closer to the ground truth throughout the entire simulation run. The simple MTM rate filter is a less accurate estimator which should only be used when no other information is available.

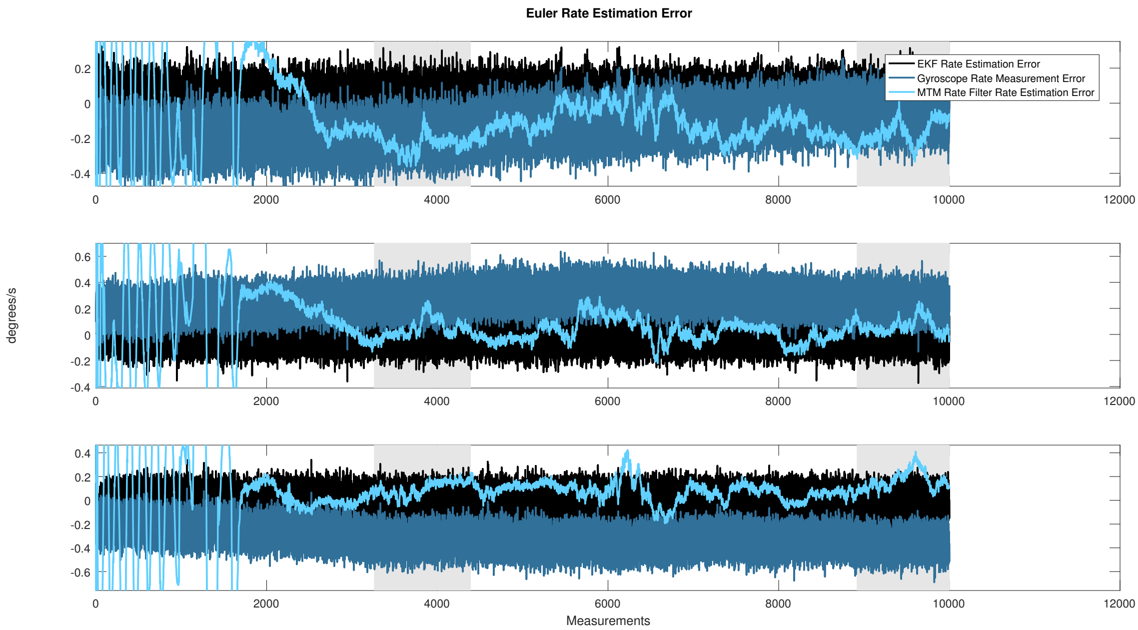

Figure 9: Rate Estimation Error

9.1.2.2 Analysis of all simulation runs

Figure 10 shows a histogram of the knowledge accuracy outside eclipse over all simulation runs in this configuration. For 50% of the time, the knowledge error remains below 0.035986 degrees. The knowledge error remains below 0.10339 degrees for 95% of the time. The lower accuracy of the star tracker around its boresight axis is reflected in a higher knowledge error around the spacecraft axis that coincides with the spacecraft optical axis.

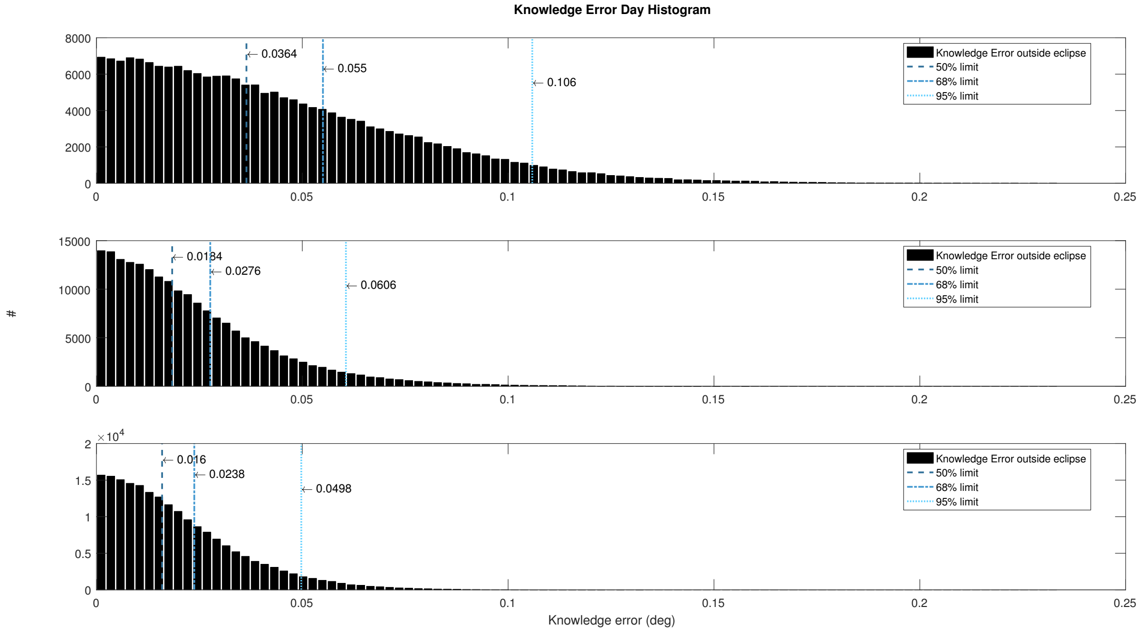

Figure 10: Histogram of the attitude knowledge error outside of eclipse

Thanks to the use of the star tracker, the knowledge error during eclipse will not differ a lot from that outside of eclipse. Figure 11 shows a histogram of the knowledge accuracy within eclipse over all simulation runs in this configuration. For 50% of the time, the knowledge error remains below 0.031825 degrees. The knowledge error remains below 0.092969 degrees for 95% of the time.

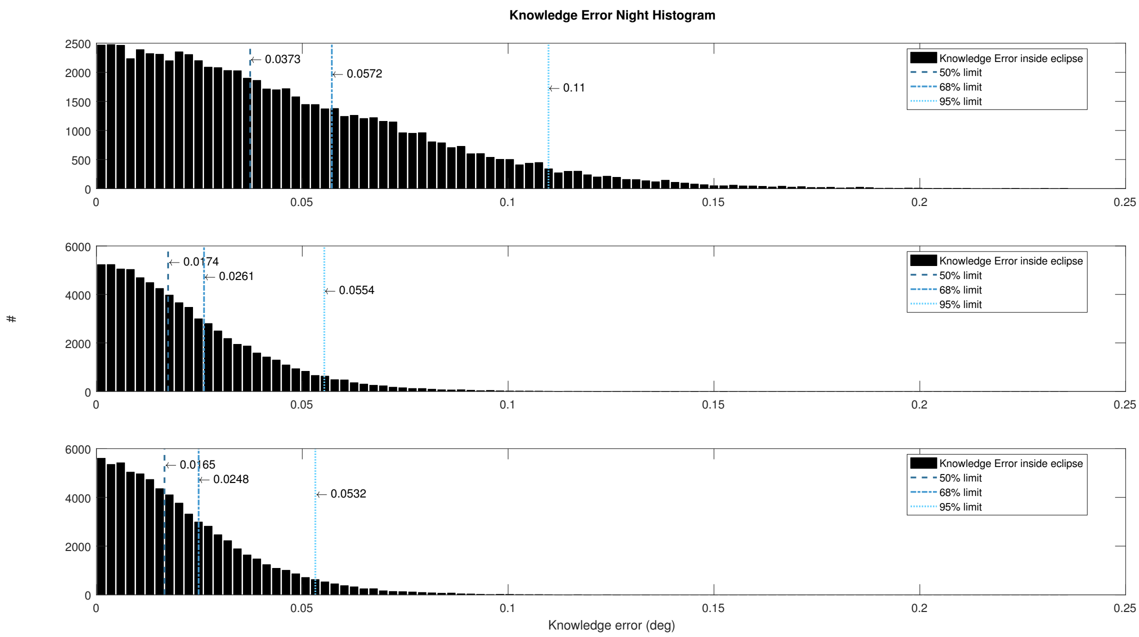

Figure 11: Histogram of the attitude knowledge error within of eclipse

9.2 POINTING PERFORMANCE

The pointing performance of the ADCS depends both on the sensors as on the actuators being used. In this document, we analyse the pointing during nominal pointing control with three RWs, but also during a fallback control law where only one RW is used. Since pointing performance also depends on the knowledge performance, we analyse the performance with and without star tracker. This leads to a total of four ADCS configurations that are analysed in the next sections.

PAGES LEFT OUT IN THE EXAMPLE DOCUMENT

9.2.1 THREE RWs WITHOUT STAR TRACKER

This ADCS configuration uses the nominal PID controller for the three RWs and uses all MTQs to desaturate the wheels. This gives the spacecraft full agile and accurate pointing control over all three axes. The lack of a star tracker will lead to deteriorating performance during eclipse. After eclipse, corrective action will need to be taken, which also negatively impacts the performance outside of eclipse.

9.2.1.1 Analysis of example simulation run

With this configuration, the attitude remains quite steady around the desired attitude (see Figure 12). In eclipse, the attitude knowledge performance reduces, which leads to higher pointing errors.

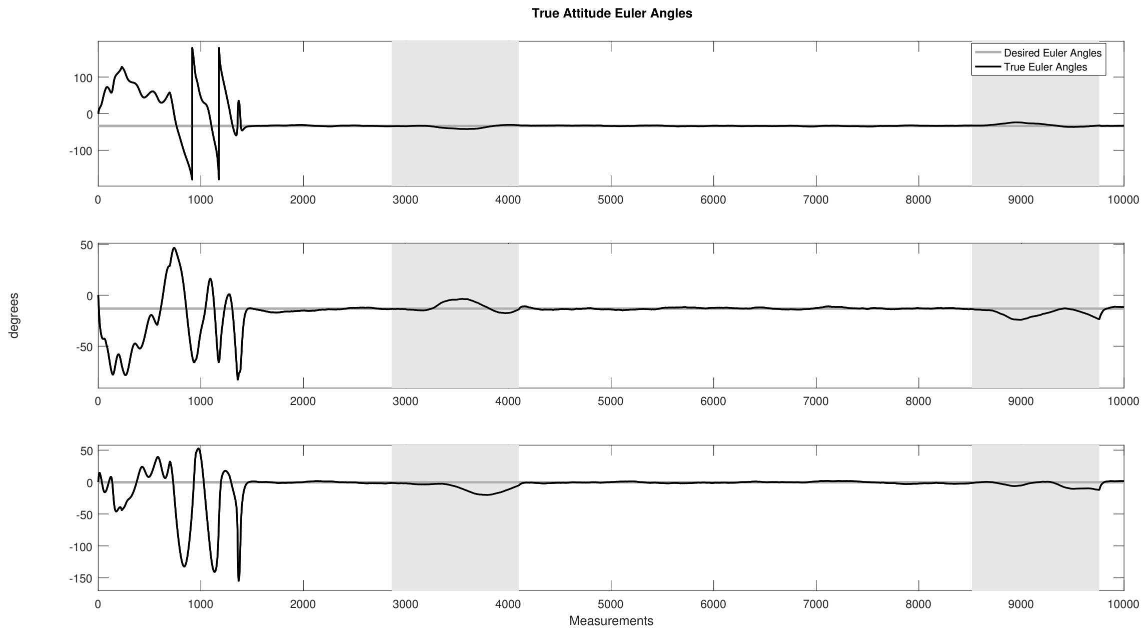

Figure 12: Attitude Euler Angles

Figure 13 shows the angular rates remaining low and stable. There is little fluctuation around the desired rotational rate. One can also observe the swift action when full attitude knowledge is regained after eclipse.

The attitude Euler Errors are shown in Figure 14. For this full control law, the pointing errors remain low around all axes.

Figure 15 shows the angular rate errors. The rates remain low and stable.
All RWs are used in these simulations. The magnetorquers desaturate the RWs so that their rotational rate would stay at a certain level, in this graph indicated by two zones in between gray lines. Figure 16 shows that the wheel speeds are kept low, which reduces power consumption.

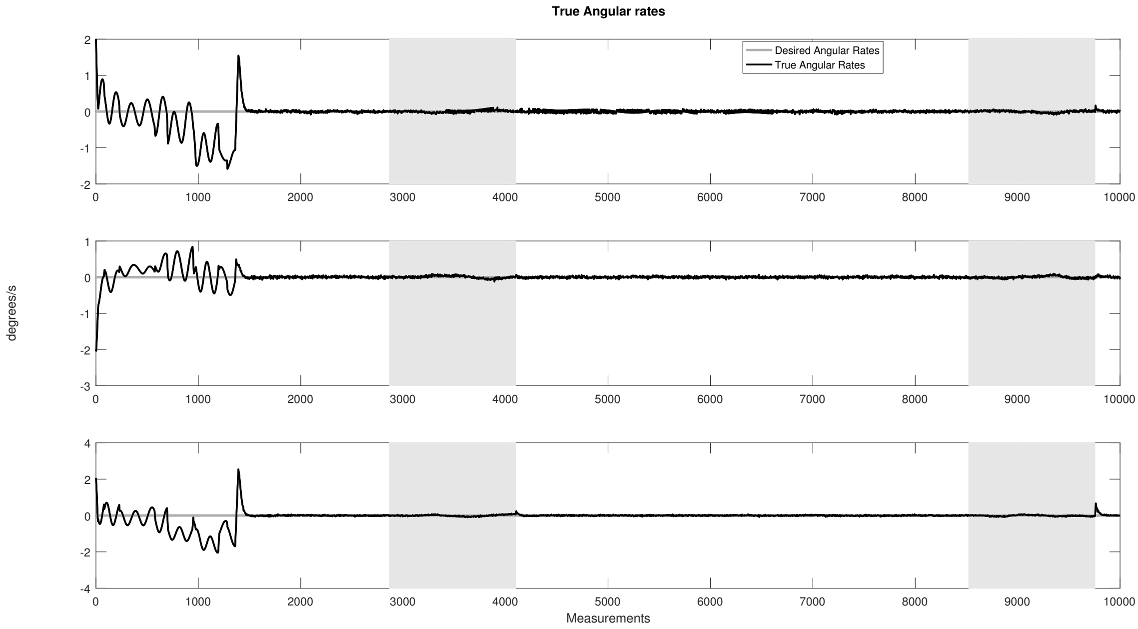

Figure 13: Angular Rates

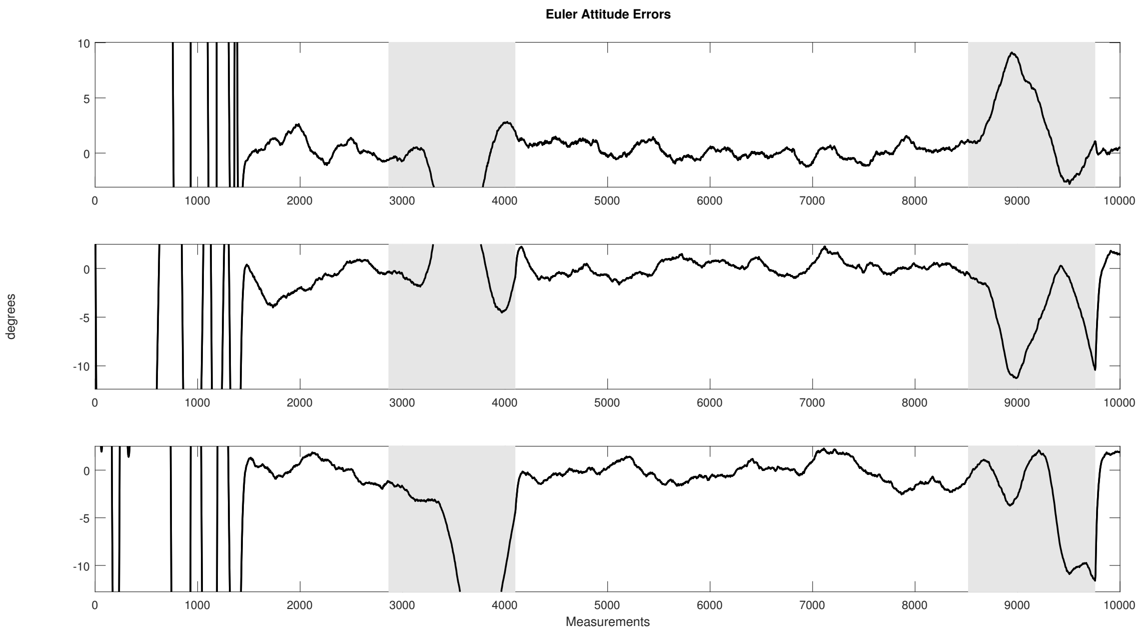

Figure 14: Attitude Euler Errors

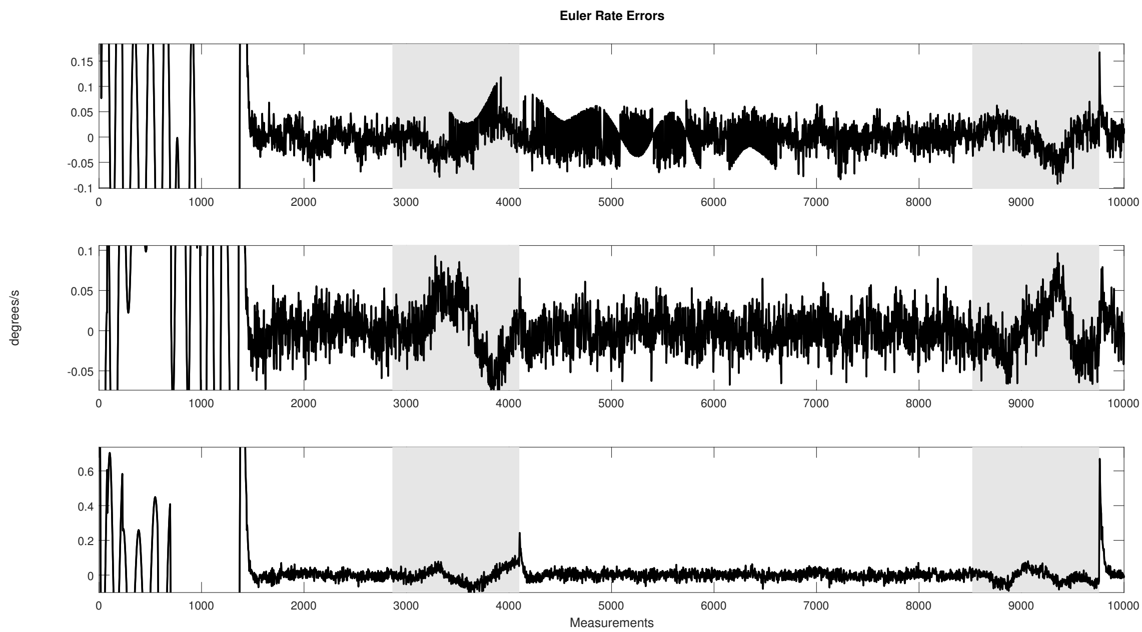

Figure 15: Angular Rate Errors

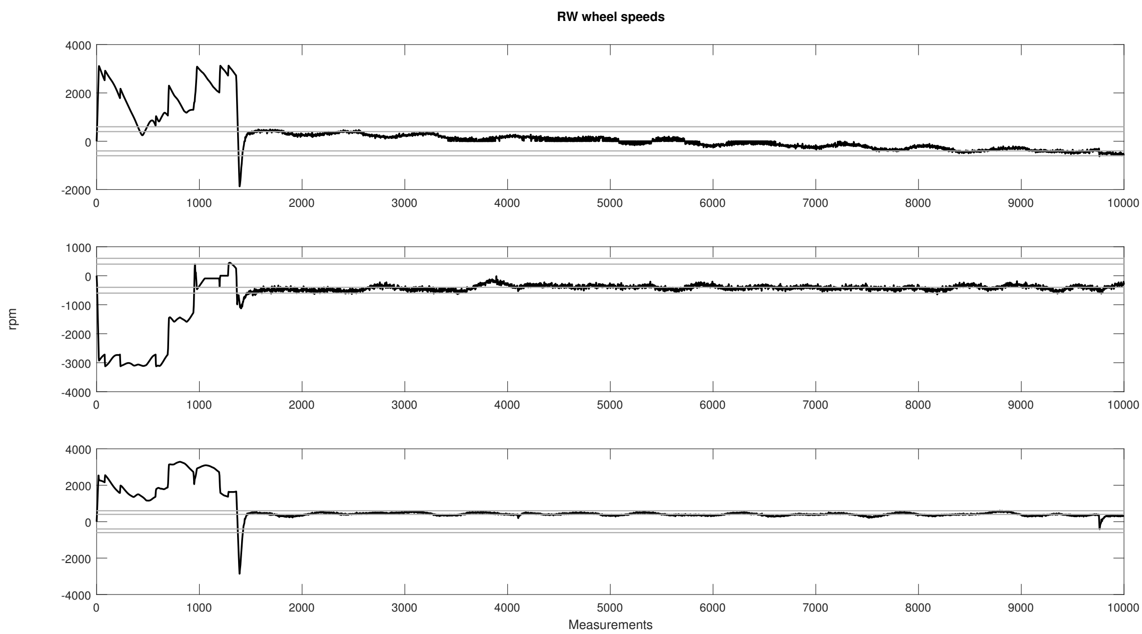

Figure 16: Reaction Wheel rotational speeds

9.2.1.2 Analysis of all simulation runs

Figure 17 shows a histogram of the pointing accuracy outside eclipse over all simulation runs in this configuration. For 50% of the time, the pointing error remains below 1.1118 degrees. The pointing error remains below 4.2595 degrees for 95% of the time.

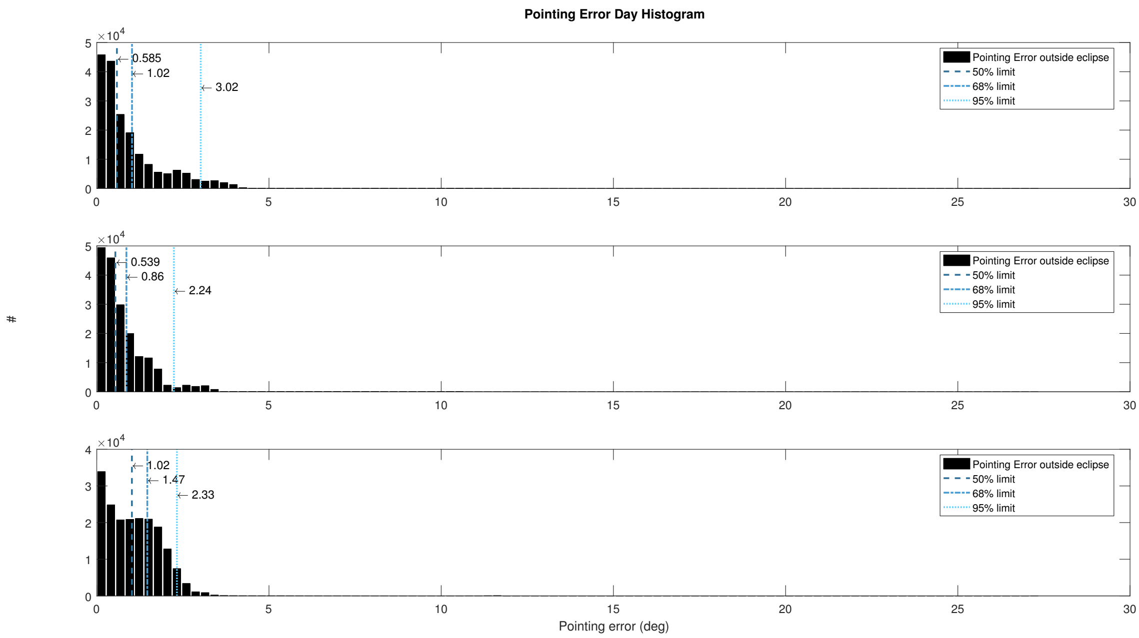

Figure 17: Histogram Pointing Error Day

Figure 18 shows a histogram of the pointing accuracy outside eclipse over all simulation runs in this configuration. For 50% of the time, the pointing error remains below 4.2033 degrees. The pointing error remains below 14.988 degrees for 95% of the time.

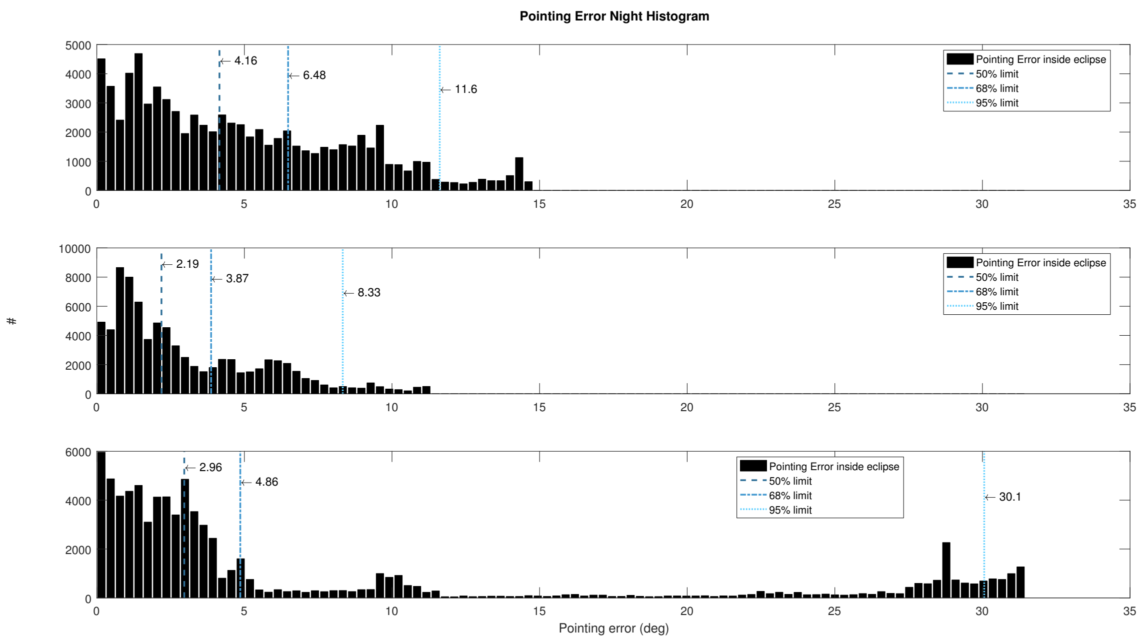

Figure 18: Histogram Pointing Error Night

one

9.2.2 THREE RWs WITH STAR TRACKER

This ADCS configuration uses the nominal PID controller for the three RWs and uses all MTQs to desaturate the wheels. This gives the spacecraft full agile and accurate pointing control over all three axes. The use of a star tracker allows full attitude knowledge during the entire simulation run. This leads to improved pointing performance.

9.2.2.1 Analysis of example simulation run

With this configuration, the attitude remains quite steady around the desired attitude (see Figure 19). The performance is the same within and outside of eclipse.

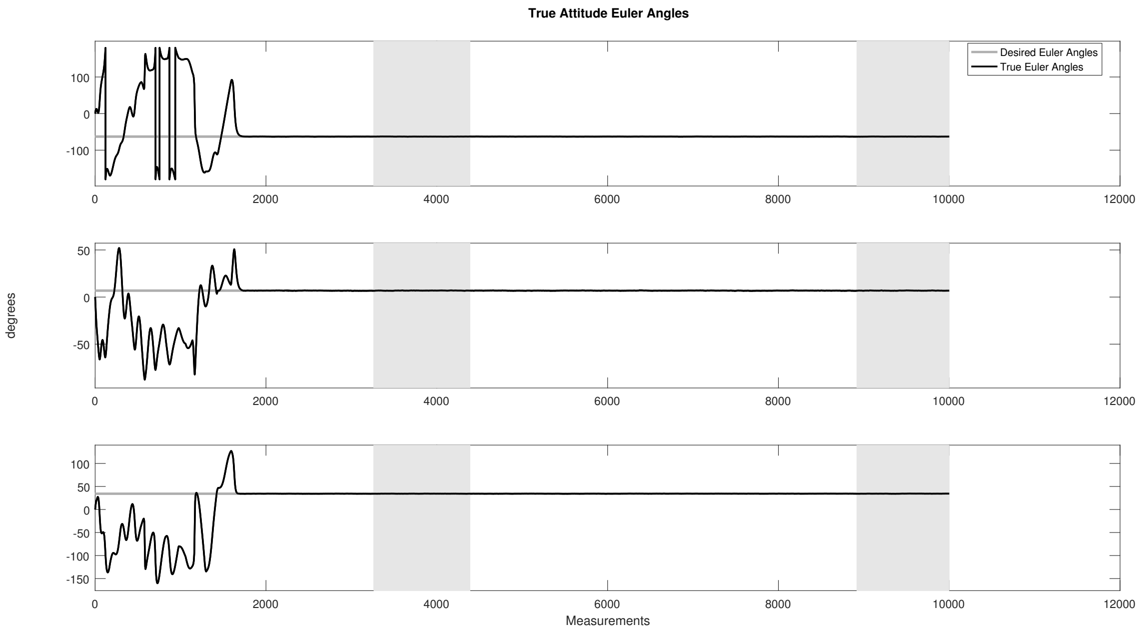

Figure 19: Attitude Euler Angles

Figure 20 shows the angular rates remaining low and stable. There is little fluctuation around the desired rotational rate.

The attitude Euler Errors are shown in Figure 21. For this full control law, the pointing errors remain low around all axes.

Figure 22 shows the angular rate errors. The rates remain low and stable.
All RWs are used in these simulations. The magnetorquers desaturate the RWs so that their rotational rate would stay at a certain level, in this graph indicated by two zones in between gray lines. Figure 23 shows that the wheel speeds are kept low, which reduces power consumption.

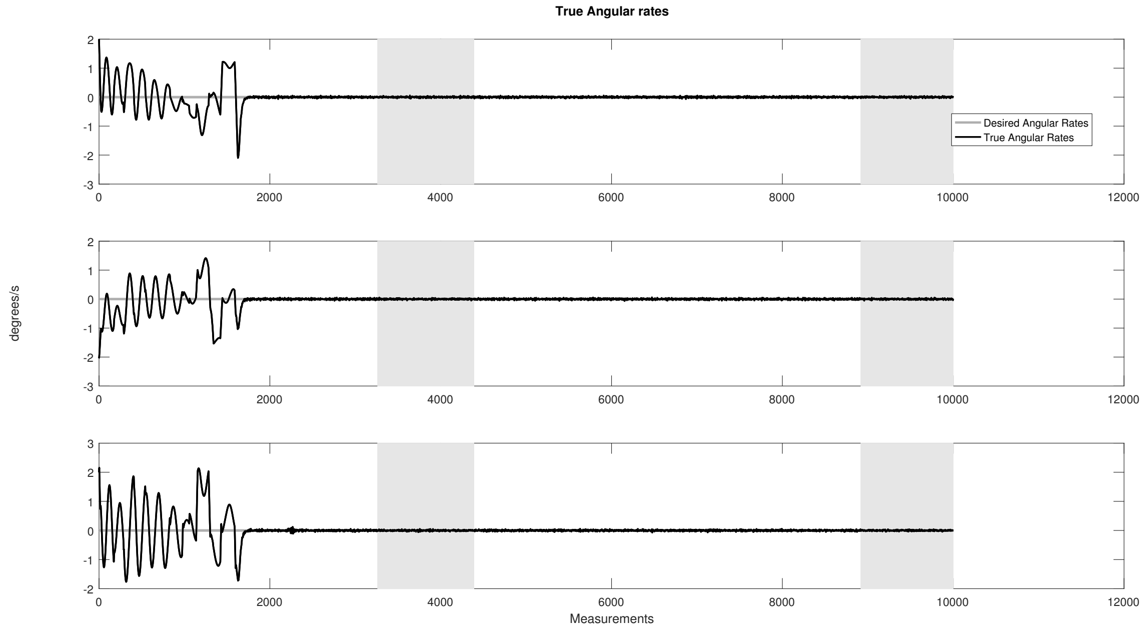

Figure 20: Angular Rates

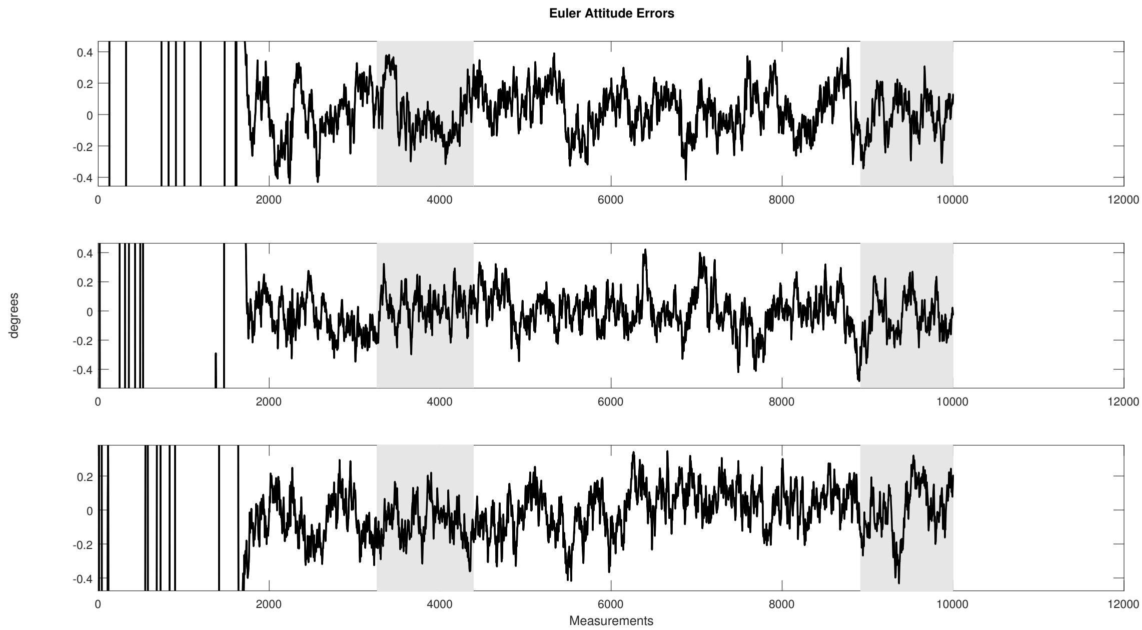

Figure 21: Attitude Euler Errors

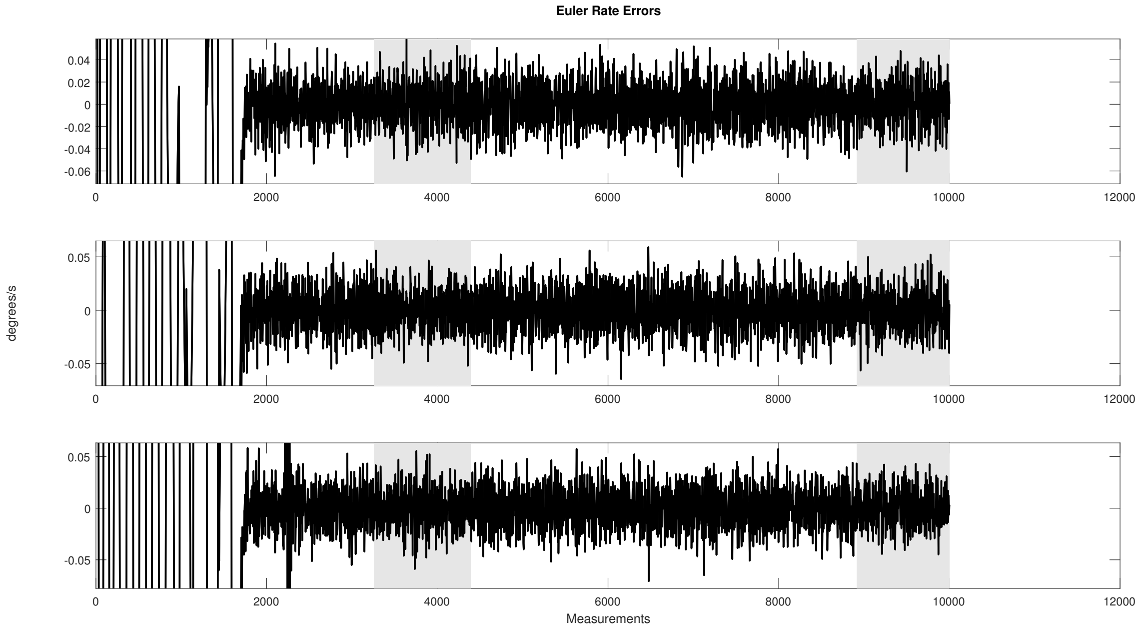

Figure 22: Angular Rate Errors

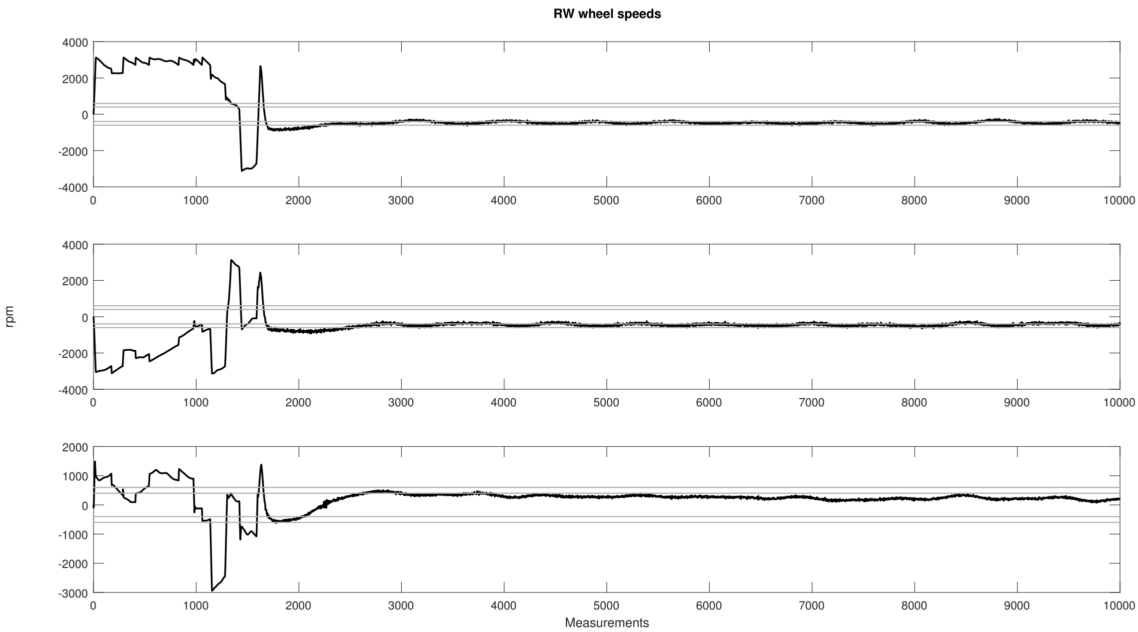

Figure 23: Reaction Wheel rotational speeds

9.2.2.2 Analysis of all simulation runs

Figure 24 shows a histogram of the pointing accuracy outside eclipse over all simulation runs in this configuration. For 50% of the time, the pointing error remains below 0.10151 degrees. The pointing error remains below 0.29854 degrees for 95% of the time.

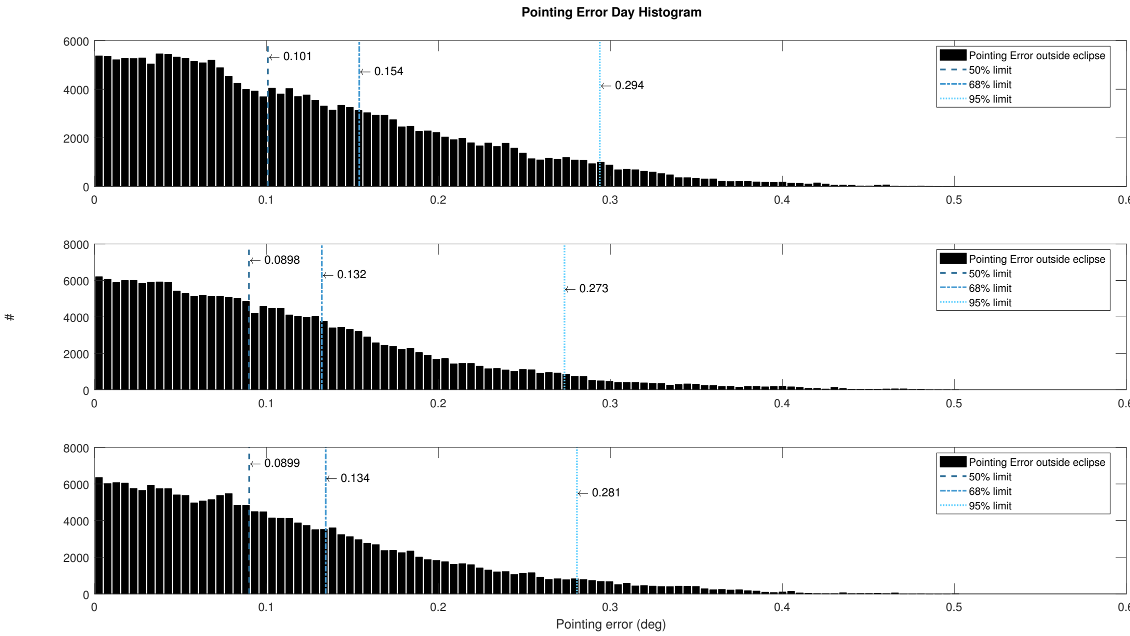

Figure 24: Histogram Pointing Error Day

Figure 25 shows a histogram of the pointing accuracy outside eclipse over all simulation runs in this configuration. For 50% of the time, the pointing error remains below 0.11019 degrees. The pointing error remains below 0.30102 degrees for 95% of the time.

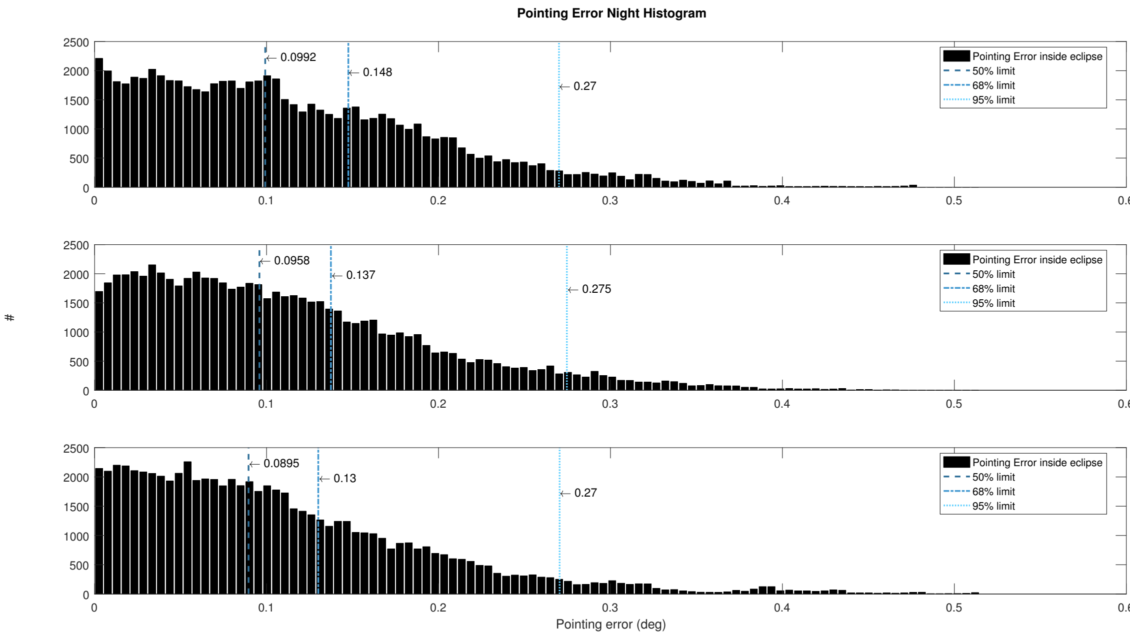

Figure 25: Histogram Pointing Error Night

9.3 POWER CONSUMPTION

PAGES LEFT OUT IN THE EXAMPLE DOCUMENT

9.3.1 3 RW, without Star Tracker

Figure 26 shows the total power consumption of the attitude determination and control system during an inertial pointing maneuver with three reaction wheels and no star tracker.

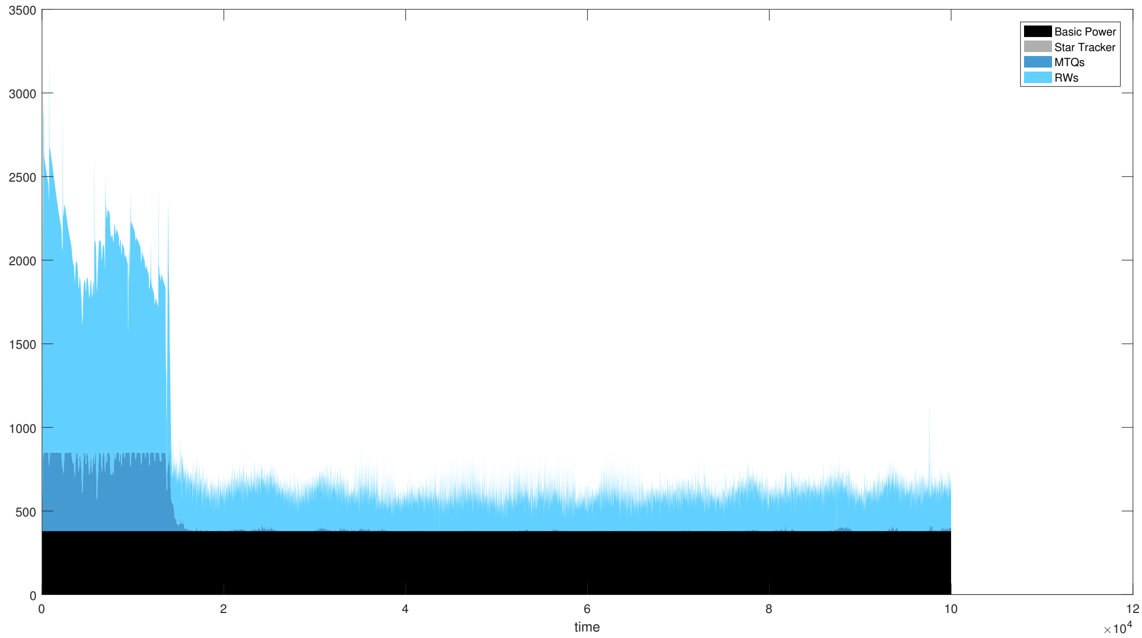

Figure 26: Total ADCS power consumption

9.3.2 3 RW, with Star Tracker

Figure 27 shows the total power consumption of the attitude determination and control system during an inertial pointing maneuver with three reaction wheels and with a star tracker.

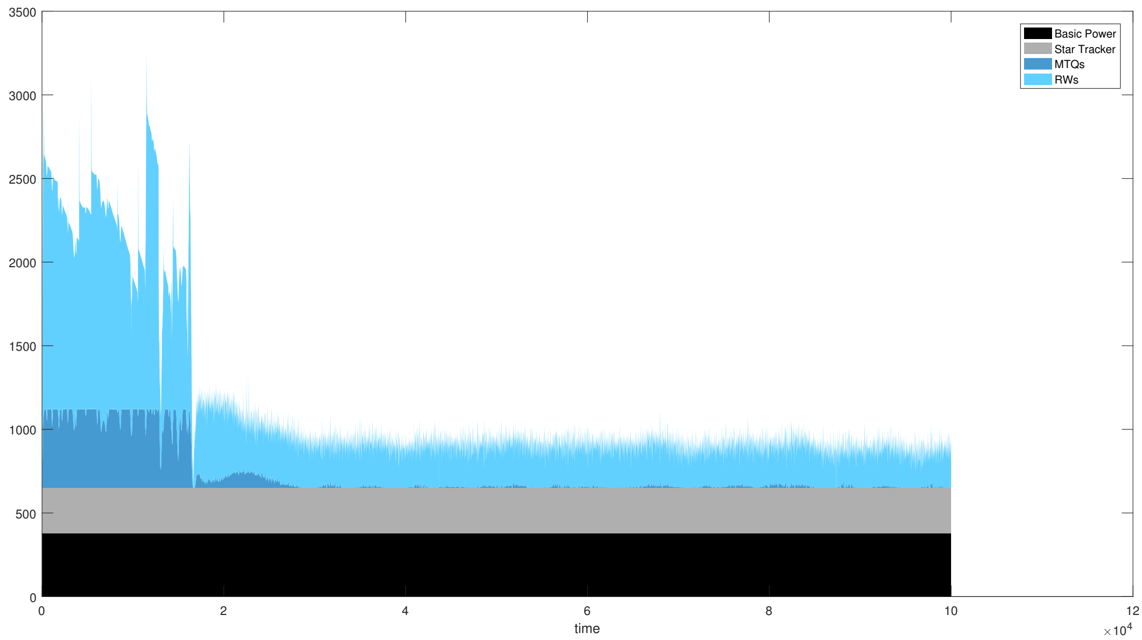

Figure 27: Total ADCS power consumption

Zenith Pointing Performance

10 3-AXIS CONTROL PERFORMANCE: ZENITH POINTING CASE

In the Zenith pointing mode, the ADCS controls the spacecraft to keep one axis pointing away from the vector towards the center of the Earth. The Zenith pointing attitude is calculated autonomously by the ADCS. These simulations start with a maneuver towards the desired attitude and the spacecraft then attempts to follow the desired attitude. As opposed to the inertial pointing case, the spacecraft needs to constantly rotate to maintain its desired attitude.

The sections below describe the knowledge performance, pointing performance and power consumption in the inertial pointing case. For each of these, Four different ADCS configurations are analysed:

- **One RW, without Star Tracker:** Using a coarse pointing algorithm which requires only one RW and the two MTQs. The star tracker is not powered on.
- **One RW, with Star Tracker:** Using a coarse pointing algorithm which requires only one RW and two MTQs. The star tracker is powered on.
- **Three RWs, without Star Tracker:** A PID-controller using all RWs and all MTQs (for desaturation) is used. The star tracker is not powered on.
- **Three RWs, with Star Tracker:** A PID-controller using all RWs and all MTQs (for desaturation) is used. The star tracker is powered on.

In nominal operation, the ADCS will use three RWs and the star tracker. The other modes are there as a fallback should a component fail. Not using the star tracker will also save power.

Most of the graphs in the next section give an example of one of the simulation runs. These serve to show the overall performance and behavior of the spacecraft in the given mode. At the end, histograms and tables give the overall results over all simulation runs and allow to assess the performance.

The graphs giving the result of one run typically show a certain characteristic (e.g. pointing error) over time. Gray areas in the graphs indicate periods of eclipse. For certain ADCS configurations, behavior inside and out of eclipse will be different.

10.1 KNOWLEDGE PERFORMANCE

The knowledge performance of the ADCS depends on the sensors being used. There will be a difference between the knowledge performance with and without use of the star tracker. The used actuators or control law do not have a significant impact. The knowledge performance is hence analysed for two different cases: with and without star tracker.

PAGES LEFT OUT IN THE EXAMPLE DOCUMENT

10.2 POINTING PERFORMANCE

The pointing performance of the ADCS depends both on the sensors as on the actuators being used. In this document, we analyse the pointing during nominal pointing control with three RWs, but also during a fallback control law where only one RW is used. Since pointing performance also depends on the knowledge performance, we analyse the performance with and without star tracker. This leads to a total of four ADCS configurations that are analysed in the next sections.

PAGES LEFT OUT IN THE EXAMPLE DOCUMENT

10.3 POWER CONSUMPTION

PAGES LEFT OUT IN THE EXAMPLE DOCUMENT

Recommendations

11 RECOMMENDATIONS

This section summarizes the simulated performance and compares it with the required performance. Based on this, some recommendations are made.

11.1 DETUMBLING

The spacecraft can reduce its detumbling rates in all five scenarios. The spacecraft should therefore be able to detumble after launch or after an anomaly.

11.2 INERTIAL POINTING

The user defined required pointing performances during Inertial pointing are given in Table 4.

Table 4: Pointing requirements during Inertial pointing

Knowledge accuracy outside eclipse		Knowledge accuracy inside eclipse	
required value	% time required	required value	% time required
0.3	95	1	95
Pointing accuracy outside eclipse		Pointing accuracy inside eclipse	
required value	% time required	required value	% time required
0.5	95	1.5	95

The pointing performance during Inertial pointing is given in table 5. The results are given for each of the control/determination modes, within and outside of eclipse. For the RMS value, we first take the root mean square over all simulation steps for each axis. Then the mean of these three RMS values gives the value in the table. The table also shows the percentage of time the simulated performance meets the requirements. The requirements are said to be met during a simulation step when the errors on all three axes remain below the required value set in table 4.

From this table, it is obvious that the star tracker greatly improves knowledge performance, while the three reaction wheels lead to more precise control.

Table 5: Pointing Performance during Inertial pointing

	Knowledge accuracy outside eclipse		Knowledge accuracy inside eclipse	
Mode	RMS value	% time met	RMS value	% time met
Three RWs, no Star Tracker	1.5629	1.1199	6.2756	9.7339
Three RWs, Star Tracker	0.036104	100	0.033528	100
	Pointing accuracy outside eclipse		Pointing accuracy inside eclipse	
Mode	RMS value	% time met	RMS value	% time met
Three RWs, no Star Tracker	1.6903	2.7151	6.5587	14.1425
Three RWs, Star Tracker	0.15101	99.6554	0.14752	100

Since only the mode using three RWs and the star tracker yields the desired performance, the simplified modes cannot be used during science operations. The recommendation is therefore to use the mode with three RWs and the star tracker at all time during operations.

11.3 ZENITH POINTING

PAGES LEFT OUT IN THE EXAMPLE DOCUMENT

12 CONCLUSION

This document described the pointing performance analysis of the Example mission. The KUL Attitude Determination and Control System is described in detail and the estimation and control algorithms are presented.

The pointing performance for Detumbling and 3-axis Pointing are analysed. For each of these, we present performance in terms of both attitude knowledge and attitude control and assess the power consumption. The results are presented and recommendations for the Example ADCS are given.
As an overall conclusion, we can say that the KUL ADCS delivers the performance required by the Example mission.

13 REFERENCES

References

[1] A. Foletti and P. Kaewkerd. Swisscube phase a adcs report. Technical report, EFPL Lausanne, Switzerland, 2006.

[2] A. Garza. Reaction wheels for picosatellites. Master's thesis, Lulea University of Technology, Sweden, 2009.

[3] Jens Giesselmann. Development of an active magnetic attitude determination and control system for picosatellites on highly inclined circular low earth orbits. Master's thesis, RMIT University, Australia, 2006.

[4] Jelle Goyvaerts. Design and implementation of a low-cost attitude determination and control system for cubesats. Master's thesis, KU Leuven, Celestijnenlaan 300B, 3001 Heverlee, Belgium, 2011.

[5] Marin Marinov and Zhivo Petrov. Allan variance analysis on error characters of low- cost mems accelerometer mma8451q. In *INTERNATIONAL CONFERENCE of SCIENTIFIC PAPER AFASES 2014*, 2014.

[6] James R. Wertz. *Spacecraft Attitude Determination and Control*. D. Reidel Publishing Company, Dordrecht, Holland, 1978. ISBN 90-277-0959-9.

[7] James R. Wertz and Wiley J. Larson. *Space Mission Analysis and Design*. Microcosm Press and Springer, Hawthorne, CA and New York NY, 3 edition, 1999.